Optical Conveyors: A Class of Active Tractor Beams

David B. Ruffner and David G. Grier

Phys. Rev. Lett. **109**, 163903 — Published 18 October 2012

DOI: 10.1103/PhysRevLett.109.163903

Optical conveyors: A class of active tractor beams

David B. Ruffner and David G. Grier
Department of Physics and Center for Soft Matter Research, New York University, New York, NY 10003
(Dated: September 20, 2012)

We experimentally demonstrate a class of tractor beams created by coherently superposing coaxial Bessel beams. These optical conveyors have periodic intensity variations along their axes that act as highly effective optical traps for micrometer-scale objects. Varying the Bessel beams' relative phase shifts the traps axially thereby selectively transports trapped objects either downstream or upstream along the length of the beam. The same methods used to project a single optical conveyor can project arrays of independent optical conveyors, allowing bi-directional transport in three dimensions.

PACS numbers: 42.50.Wk, 42.40.-i, 82.70.Dd

A tractor beam is a traveling wave that can transport illuminated material along its length back to its source. By this definition, an optical tweezer [1] is not a tractor beam because of its inherently limited range. Nor is an optical conveyor belt [2, 3], which is created from a standing wave rather than a traveling wave. A one-sided variant of the optical conveyor belt created from coaxial Bessel beams has been demonstrated, but relies on auxiliary forces to achieve retrograde motion [4]. Here, we demonstrate one-sided optical conveyors that act as tractor beams without requiring outside assistance. The same technique we use to project a single optical conveyor also can project arrays of optical conveyors each with independently controlled transport properties.

Most beams of light do not act as tractor beams because radiation pressure tends to drive illuminated objects downstream. Recently, however two categories of tractor beams have been described, both of which exploit properties of propagation-invariant or non-diffracting traveling waves [5], and thus have promise for long-range material transport. Both rely on the recoil force that an illuminated object experiences if it scatters transverse components of the beam's linear momentum density into the axial direction. The first is based on multipole scattering in Bessel beams, which has been predicted to drive retrograde motion in both acoustic [6] and optical [7] waves. Because this mechanism relies on scattering by high-order induced multipole moments, however, the direction of induced transport depends sensitively on the properties of the illuminated object; tractor beams based on pure Bessel modes have not yet been demonstrated experimentally. The other approach utilizes periodic axial intensity gradients in beams with discrete propagation invariance [5] to achieve forward scattering from the interference between the incident field and the dipole radiation field of an illuminated object. Such tractor beams have been realized experimentally with solenoidal waves that have transported micrometer-scale colloidal spheres over an axial range of 10 μm [8].

Here, we describe another category of tractor beams derived from the optical conveyor belts introduced in Refs. [2–4] that can be projected from a single source and can transport material bidirectionally without the aid of outside forces. A one-sided optical conveyor is formed by projecting two or more coherent Bessel beams along the same axis and systematically varying their relative phase. The vector potential for a two-component optical conveyor of frequency ω and polarization $\hat{\epsilon}$ may be written in cylindrical coordinates $\mathbf{r} = (r, \theta, z)$ as

$$\mathbf{A}_m(\mathbf{r}, t) = A_m \left\{ J_m\left(\left[1-\alpha^2\right]^{\frac{1}{2}} kr\right) e^{i\,\alpha kz} + \eta\, e^{i\varphi(t)}\, J_m\left(\left[1-\beta^2\right]^{\frac{1}{2}} kr\right) e^{i\,\beta kz} \right\} e^{im\theta}\, e^{-i\omega t}\, \hat{\epsilon}, \quad (1)$$

where $k = n_m\omega/c$ is the wavenumber of light in a medium with refractive index n_m and $J_m(\,\cdot\,)$ is a Bessel function of the first kind of order m. The two beams differ in their axial wavenumbers, αk and βk, which are reduced from k by factors $\alpha, \beta \in (0, 1)$. They also differ in their relative phase $\varphi(t)$, whose time variation makes the conveyor work. The prefactor A_m is the beam's amplitude. Setting the relative amplitude to unity, $\eta = 1$, maximizes the conveyor's axial intensity gradients and thus optimizes its performance for optical manipulation.

In the special case $m = 0$, $\eta = 1$, the component Bessel beams have unit amplitude along the optical axis, $r = 0$, and the conveyor's axial intensity is

$$\lim_{r\to 0} I(\mathbf{r}, t) = \frac{1}{2}\, cn_m\epsilon_0\omega^2 \lim_{r\to 0} |\mathbf{A}_0(\mathbf{r}, t)|^2 \quad (2)$$

$$= I_0 \cos^2\left(\frac{1}{2}\left[(\alpha-\beta)\, kz - \varphi(t)\right]\right), \quad (3)$$

where $I_0 = 2A_0^2 cn_m\epsilon_0\omega^2$. The beam thus has intensity maxima at axial positions

$$z_j(t) = \left[j + \frac{\varphi(t)}{2\pi}\right] \Delta z \quad (4)$$

that are evenly spaced by multiples, $\Delta z = \lambda/(\alpha-\beta)$, of the wavelength $\lambda = 2\pi/k$ in the medium, and thus can be indexed by the integer j.

Objects trapped along $I(z, t)$ can be displaced either up or down the axis by appropriately varying the relative phase $\varphi(t)$. Continuous variations translate trapped

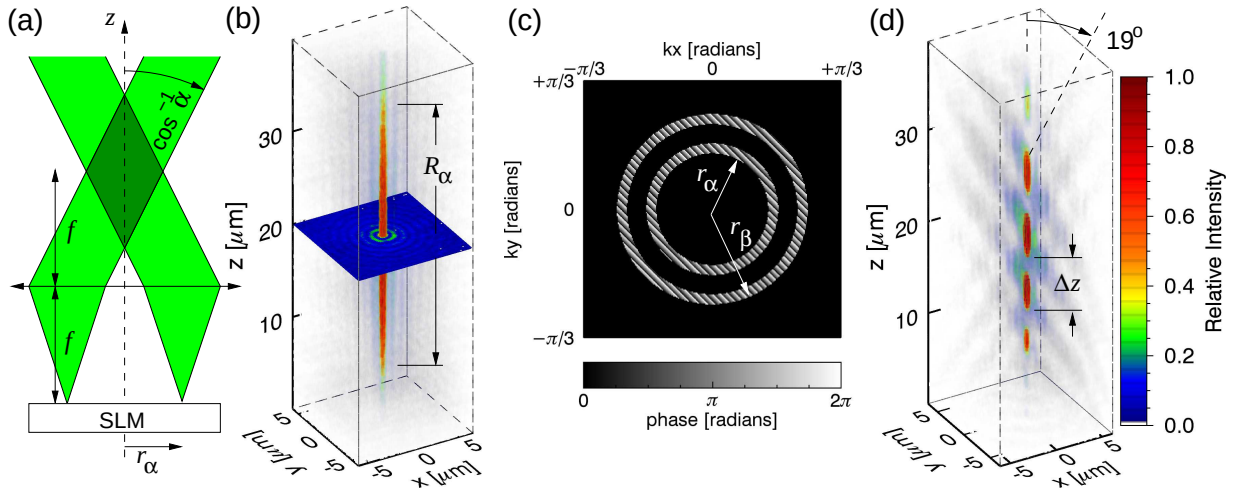

FIG. 1. (color online) (a) Schematic representation of holographic projection of a Bessel beam with axial wavenumber αk by a lens of focal length f. Shaded region indicates volume of invariant propagation. (b) Volumetric reconstruction of a holographically projected Bessel beam. (c) Phase hologram encoding an optical conveyor. Diagonal blazing tilts the projected conveyor away from the optical axis. (d) Volumetric reconstruction of the beam projected by the hologram in (c). The color bar indicates relative intensities in (b) and (d).

objects deterministically along $\hat{z}$ with axial velocity,

$$v(t) = \Delta z \frac{\partial_t \varphi(t)}{2\pi} \tag{5}$$

regardless of their size, shape, or optical properties. This differs from the action of Bessel-based tractor beams [6] in which even the sign of the induced motion depends on each object's properties. It differs also from the motion induced by solenoidal tractor beams [8] which is unidirectional but not uniformly fast.

We implemented optical conveyors using the holographic optical trapping technique [9] in which a computer-designed phase profile is imprinted onto the wavefronts of a Gaussian beam, which then is projected into the sample with a high-numerical-aperture objective lens of focal length f. In practice, the trap-forming hologram is implemented with a computer-addressable spatial light modulator (SLM) (Hamamatsu X8267-16) that imposes a selected phase shift at each pixel in a 768×768 array. If the field described by Eq. (1) is to be projected into the objective's focal plane, the field in the plane of the hologram is given in the scalar diffraction approximation [10] by its Fourier transform,

$$\tilde{\mathbf{A}}_m(\mathbf{r},t) = i^{m+1} \frac{f}{k} A_m e^{im\theta} e^{-i\omega t} \times \left[\frac{1}{r_\alpha} \delta(r - r_\alpha) + \eta e^{i\varphi(t)} \frac{1}{r_\beta} \delta(r - r_\beta) \right] \hat{\epsilon}, \tag{6}$$

where $\delta(\cdot)$ is the Dirac delta function, $r_\alpha = f(1-\alpha^2)^{\frac{1}{2}}$ and $r_\beta = f(1-\beta^2)^{\frac{1}{2}}$, The ideal hologram for each Bessel beam comprising the conveyor thus is a thin ring in the plane of the SLM, as indicated schematically in Fig. 1(a). A holographically projected Bessel beam then propagates without diffraction over the range indicated by the shaded region. Increasing the transverse wave number increases the radius of the hologram and therefore reduces the non-diffracting range.

Figure 1(b) shows a volumetric reconstruction [11] of a Bessel beam projected with a ring-like hologram. Increasing the ring's thickness of the ring by $\pm\Delta r$ increases diffraction efficiency, but is equivalent to superposing Bessel beams with a range of axial wavenumbers, $\Delta\alpha = r_\alpha \Delta r_\alpha / (\alpha f^2)$. This superposition contributes an overall axial envelope to the projected Bessel beam, limiting its axial range to $R_\alpha = 2\lambda/\Delta\alpha$. The axial range in Fig. 1(b) is consistent with this estimate and so is smaller than the ray-optics estimate suggested by the overlap volume in Fig. 1(a).

Figure 1(c) shows the two-ringed phase-only hologram that encodes an optical conveyor with an overall cone angle of $\cos^{-1}([\alpha+\beta]/2) = 19°$. This function corresponds to the phase of the beam's vector potential, which the SLM imprints on an incident Gaussian plane wave. The relative phase offset between the two rings determines $\varphi(t)$. The relative widths of the two phase rings can be used to establish the components' relative amplitudes through $\eta = r_\beta^2 \Delta r_\beta / (r_\alpha^2 \Delta r_\alpha)$, the range of the projected conveyor then being the smaller of R_α and R_β.

The large featureless regions in Fig. 1(c) do not contribute to the desired optical conveyor. Light passing through these regions is not diffracted and therefore converges at the focal point of the optical train. To prevent interference between the diffracted and undiffracted beams, the two phase rings contributing to the conveyor are offset and blazed with a linear phase gradient [12] to

displace the projected Bessel beams by 24 μm from the optical axis.

The volumetric reconstruction in Fig. 1(d) shows the three-dimensional intensity distribution projected by the hologram in Fig. 1(c), with $\hat{z}$ oriented along the diffracted beam's direction of propagation. This beam clearly displays the pattern of periodically alternating bright and dark regions predicted by Eqs. (1) through (4).

The unused regions of the hologram need not go to waste. They can be used to project additional independent conveyors, much as has been demonstrated for spatially multiplexed optical traps of other types [13]. An appropriately designed array of conveyors therefore can make full use of the light falling on the SLM and thus can be projected with very high diffraction efficiency. Each conveyor, moreover, can be operated independently of the others by selectively offsetting the phase in appropriate regions of the multiplexed hologram.

The data in Fig. 2 were obtained with two separate optical conveyors projected simultaneously with equal intensity and equal axial period by a single hologram. The conveyors' phases were ramped at the same rate, but with opposite sign. This single structured beam of light therefore should transport material in opposite directions simultaneously. To demonstrate this, we projected the pair of conveyors into a sample of 1.5 μm diameter colloidal silica spheres dispersed in water (Polysciences, Lot # 600424). The sample is contained in the 100 μm deep gap between a clean glass microscope slide and a coverslip that was formed by and sealed with UV-curing optical adhesive (Norland 68). The slide was mounted on the stage of a Nikon TE-2000U optical microscope outfitted with a custom-built holographic optical trapping system [14] operating at a vacuum wavelength of $\lambda_0 = 532$ nm. An estimated 17 mW of linearly polarized light were projected into each conveyor with a 100× numerical aperture 1.4 oil-immersion objective lens (Nikon Plan-Apo DIC H) at an overall efficiency of 0.5 percent.

To facilitate tracking the spheres as they move along the optical axis, the microscope's conventional illuminator was replaced with a 10 mW 3 mm-diameter collimated laser beam at a vacuum wavelength of 445 nm. Interference between light scattered by the spheres and the rest of the illumination forms a hologram of the spheres in the focal plane of the objective lens that is magnified and recorded at 30 frames per second with a conventional greyscale video camera (NEC TI-324A-II). A typical holographic snapshot is reproduced in Fig. 2(a). These holograms then can be analyzed [15, 16] to obtain the spheres' three-dimensional positions with nanometer-scale resolution. The traces in Fig. 2(a) show the full trajectories of both spheres over the course of the experiment. Colored orbs indicate the measured positions of the spheres at the instant of the holographic snapshot and are scaled to represent the actual sizes of the spheres. Starting from the configuration in Fig. 2(a), the two conveyors were run through total phase ramps of $\pm 10\pi$ rad in steps of $\pi/4$ rad, yielding the axial trajectories plotted in Fig. 2(b). Reversing the phase ramps reverses the process [17]. These measurements confirm that arrays of optical conveyors can selectively induce bidirectional transport over their entire lengths.

The self-healing nature of Bessel beams [5, 18] furthermore suggests that multiple objects can be trapped and moved by a single optical conveyor despite light scattering by each of the trapped objects [2–4]. This is confirmed by Fig. 2(c), which shows a volumetric reconstruction [15, 19] of the light scattered by two colloidal spheres simultaneously trapped on an optical conveyor. The plotted intensity distribution was computed from the inset hologram by Rayleigh-Sommerfeld back-propagation. Maxima representing the positions of the spheres are separated by two periods of the underlying optical conveyor.

To characterize and optimize the transport properties of optical conveyors, we model the forces they exert in the Rayleigh approximation, which is appropriate for objects smaller than the wavelength of light. Considering both induced-dipole attraction and radiation pressure, the axial component of the force is

$$F(z,t) = a\,\partial_z I(\mathbf{r},t) + b\,I(\mathbf{r},t), \tag{7}$$

where the coefficients $a = \Re\{\alpha_e\}/(4\epsilon_0 c)$ and $b = \Im\{\alpha_e\}(\alpha+\beta)k/(4\epsilon_0 c)$ parameterize the light-matter interaction for a particle with electric polarizability α_e. For simplicity, Eq. (7) omits contributions due to the curl of the spin density [20], and thus is appropriate for linearly polarized light. Further assuming a conveyor of the form described by Eq. (2) with continuously ramped phase, $\varphi(t) = \Omega t$, the equation of motion for a colloidal particle with drag coefficient γ is

$$\frac{\dot{z}(t)}{u_0} = \sqrt{1+\xi^2}\sin\left(2\pi\frac{z(t)}{\Delta z} + \Omega t - \cot^{-1}\xi\right) + 1, \tag{8}$$

where $u_0 = I_0 b/(2\gamma)$ is the downstream drift speed due to radiation pressure, and where $\xi = 2\pi a/(b\,\Delta z)$ describes the relative axial trapping strength. Particles that are trapped by intensity gradients are translated upstream with the conveyor's phase velocity, $\dot{z}(t) = -v_0 = -\Delta z\,\Omega/(2\pi)$. From Eq. (8), the maximum upstream transport speed is then limited by viscous drag to

$$v_0 \le u_0\sqrt{1+\xi^2} - u_0 = \frac{I_0 b}{2\gamma}\left[\sqrt{1+\left(\frac{2\pi a}{b\Delta z}\right)^2} - 1\right]. \tag{9}$$

This remarkable result suggests that an optical conveyor can act as a tractor beam for any particle with $|a| > 0$ provided that it is not run too fast. Both light-seeking ($a > 0$) and dark-seeking ($a < 0$) particles should move in the same direction with the same speed, although the dark-seeking particles will sit near the beam's minima.

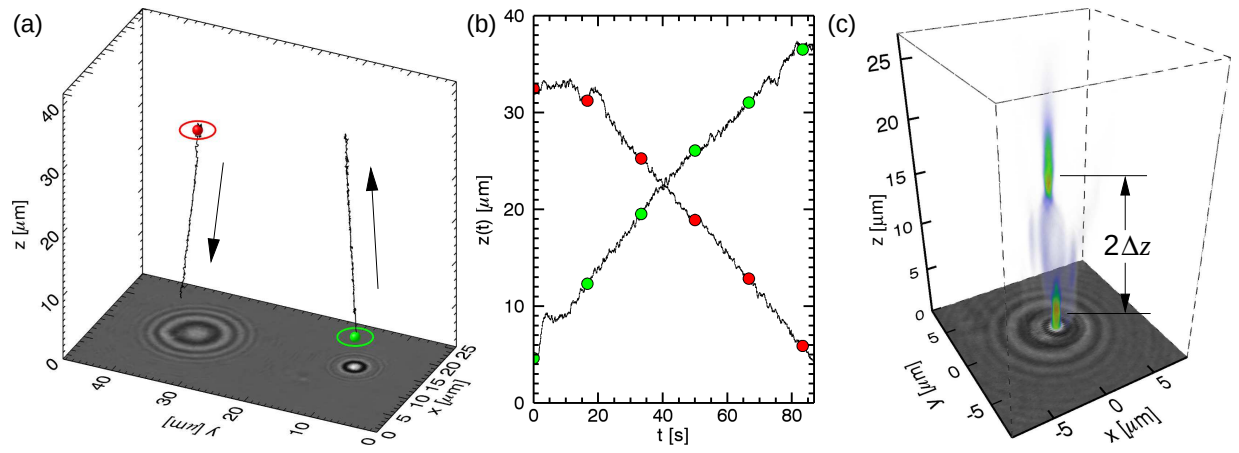

FIG. 2. (color online) (a) Trajectories of two 1.5 μm diameter colloidal silica spheres moving along a pair of optical conveyors, superimposed with a holographic snapshot of the two spheres. Colored orbs indicate the spheres' positions in the hologram, and are plotted at the same scale as the actual spheres. Rings are added for emphasis. (b) Measured time dependence of the spheres' axial positions as one moves downstream ($+\hat{z}$) along its conveyor and the other moves upstream ($-\hat{z}$). (c) Three-dimensional reconstruction of a holographic snapshot of two colloidal spheres moving along a single optical conveyor.

Optical conveyors thus have the potential to out-perform optical tweezers, which cannot always achieve stable axial trapping even in the Rayleigh regime.

Equation (9) also suggests straightforward optimization strategies for optical conveyors. Brighter conveyors can run faster. Reducing the conveyor's spatial period Δz proportionately increases the maximum transport rate at the cost of reducing the maximum range.

Higher-order conveyors with $m > 0$ also have intensity maxima at positions z_j given by Eq. (4). They differ from zero-order conveyors in that their principal maxima are displaced from $r = 0$ to transverse radii that depend on m, α, and β. This larger transverse range may be useful for conveying irregular or asymmetrically shaped objects, or objects with inhomogeneous optical properties. Higher-order conveyors also carry orbital angular momentum and so will exert torques on trapped objects.

The transport direction predicted by Eq. (8) reverses sign in the limit of large Ω, illuminated objects then traveling steadily downstream at the drift speed u_0. The crossover between upstream and downstream transport is marked by a dynamical state in which the particle alternately is transported upstream and slips back downstream. The transition to this state is established by Eq. (9) in the deterministic case described by Eq. (8). It will be strongly affected by thermal fluctuations, however, and may feature anomalous velocity fluctuations. Still other dynamical states are possible if the relative phase $\varphi(t)$ varies discontinuously, for example in a Brownian ratchet protocol [21]. Even more complicated behavior may be expected for optical conveyor transport in underdamped systems for which inertia plays a role.

This work was supported by the National Science Foundation under Grant Number DMR-0922680. The authors are grateful for enlightening conversations with Paul Stysley, Demetrios Poulios and Donald Coyle.

[1] A. Ashkin, J. M. Dziedzic, J. E. Bjorkholm, and S. Chu, Opt. Lett. **11**, 288 (1986)

[2] T. Čižmar, V. Garcés-Chávez, K. Dholakia, and P. Zemánek, Appl. Phys. Lett. **86**, 174101 (2005).

[3] T. Čižmár, M. Šiler, and P. Zemánek, Appl. Phys. B **84**, 197 (2006).

[4] T. Čižmár, V. Kollárová, Z. Bouchal, and P. Zemánek, New J. Phys. **8**, 43 (2006).

[5] J. Durnin, J. J. Miceli, Jr., and J. H. Eberly. Phys. Rev. Lett. **58**, 1499 (1987).

[6] P. L. Marston, J. Acoust. Soc. Am. **120**, 3518 (2006).

[7] J. Chen, J. Ng, Z. Lin, and C. T. Chan, Nature Photonics **5**, 531 (2011).

[8] S.-H. Lee, Y. Roichman, and D. G. Grier, Opt. Express **18**, 6988 (2010).

[9] E. R. Dufresne and D. G. Grier, Rev. Sci. Instrum. **69**, 1974 (1998); D. G. Grier, Nature **424**, 810 (2003).

[10] J. W. Goodman, *Introduction to Fourier Optics*, 3rd ed. (McGraw-Hill, New York, 2005).

[11] Y. Roichman, I. Cholis, and D. G. Grier, Opt. Express **14**, 10907 (2006).

[12] J. E. Curtis, B. A. Koss, and D. G. Grier, Opt. Commun. **207**, 169 (2002).

[13] C.-S. Guo, X. Liu, J.-L. He, and H.-T. Wang, Opt. Express **12**, 4625 (2004);; K. Ladavac and D. G. Grier, Europhys. Lett. **70**, 548 (2005);; Y. Roichman and D. G. Grier, Opt. Lett. **31**, 1675 (2006).

[14] M. Polin, K. Ladavac, S.-H. Lee, Y. Roichman, and D. G. Grier, Opt. Express **13**, 5831 (2005).

[15] S.-H. Lee, Y. Roichman, G.-R. Yi, S.-H. Kim, S.-M. Yang, A. van Blaaderen, P. van Oostrum, and D. G. Grier, Opt. Express **15**, 18275 (2007);; F. C. Cheong, B. J. Krishnatreya, and D. G. Grier, *ibid.* **18**, 13563 (2010).

[16] F. C. Cheong, B. Sun, R. Dreyfus, J. Amato-Grill, K. Xiao, L. Dixon, and D. G. Grier, Opt. Express **17**, 13071 (2009).

[17] See EPAPS Document No. [number will be inserted by publisher] for a video of this transport process. For more information on EPAPS, see `http://www.aip.org/pubservs/epaps.html`.

[18] V. Garcés-Chávez, D. McGloin, H. Melville, W. Sibbett, and K. Dholakia, Nature **419**, 145 (2002).

[19] S.-H. Lee and D. G. Grier, Opt. Express **15**, 1505 (2007).

[20] S. Albaladejo, M. I. Marqués, F. Scheffold, and J. J. Sáenz, Nano Lett. **9**, 3527 (2009);; D. B. Ruffner and D. G. Grier, Phys. Rev. Lett. **108**, 173602 (2012).

[21] S.-H. Lee, K. Ladavac, M. Polin, and D. G. Grier, Phys. Rev. Lett. **94**, 110601 (2005);; S.-H. Lee and D. G. Grier, Phys. Rev. E **71**, 060102(R) (2005);; J. Phys.: Condens. Matter **17**, S3685 (2006).